

PSO-Based Optimal Coverage Path Planning for Surface Defect Inspection of 3C Components with a Robotic Line Scanner

Hongpeng Chen¹, Shengzeng Huo¹, Muhammad Muddassir²,
Hoi-Yin Lee¹, Anqing Duan¹, Pai Zheng¹, Hongsheng Pan³,
David Navarro-Alarcon^{1*}

¹*Faculty of Engineering, The Hong Kong Polytechnic University,
Kowloon, Hong Kong.

²Faculty of Construction and Environment, The Hong Kong Polytechnic University, Kowloon, Hong Kong.

³Shanghai Microintelligence Technology Co. Ltd, Shanghai, China.

*Corresponding author(s). E-mail(s): dnavar@polyu.edu.hk;
Contributing authors: holychp.chen@connect.polyu.hk;
kyle-sz.huo@connect.polyu.hk; mmudda@polyu.edu.hk;
hoi-yin.lee@connect.polyu.hk; aduan@polyu.edu.hk;
pai.zheng@polyu.edu.hk; hongsheng.pan@micro-i.com.cn;

Abstract

The automatic inspection of surface defects is an important task for quality control in the computers, communications, and consumer electronics (3C) industry. Conventional devices for defect inspection (viz. line-scan sensors) have a limited field of view, thus, a robot-aided defect inspection system needs to scan the object from multiple viewpoints. Optimally selecting the robot's viewpoints and planning a path is regarded as coverage path planning (CPP), a problem that enables inspecting the object's complete surface while reducing the scanning time and avoiding misdetection of defects. However, the development of CPP strategies for robotic line scanners has not been sufficiently studied by researchers. To fill this gap in the literature, in this paper, we present a new approach for robotic line scanners to detect surface defects of 3C free-form objects automatically. Our proposed solution consists of generating a local path by a new hybrid region segmentation method and an adaptive planning algorithm to ensure the coverage of the complete object surface. An optimization method for the global path

sequence is developed to maximize the scanning efficiency. To verify our proposed methodology, we conduct detailed simulation-based and experimental studies on various free-form workpieces, and compare its performance with a state-of-the-art solution. The reported results demonstrate the feasibility and effectiveness of our approach.

Keywords: Coverage path planning (CPP), Line-scan sensor, Surface inspection, Robotic inspection, 3C components

1 Introduction

Defect inspection is essential to quality control, process monitoring, and non-destructive testing (NDT) in the manufacturing industry (Chen et al., 2022; Chen & Yang, 2021; Luo & He, 2016). Specifically, manufacturing processes in the 3C industry are highly sophisticated and demand detailed and accurate defect inspection. Traditional defect inspection approaches typically rely on visual inspection of an intermediate/finished product by a quality control or quality check inspector. This sole dependence on human workers is a problem for regions and countries with a shortage of manpower (Liu et al., 2022; Ming et al., 2020). Furthermore, human-based inspection is inherently subjective, hence, prone to errors. To address these problems, various researchers have reported the automatic surface inspection system for free-form components (Li et al., 2023; Yang et al., 2023).

Recently, automatic detection systems equipped with an industrial-grade line scanner, depth camera, and robotic manipulator has been developed to offer effective and rapid non-contact measurement (Huo et al., 2022; Liu et al., 2022). During the defect inspection task, the robotics inspection system scans the surface of the target workpiece exhaustively from different viewpoints. Planning an inspection path can be considered as the CPP problem (Molina et al., 2017). Estimating a CPP strategy for automatic inspection consists of three tasks: (1) determining the viewpoints to measure the workpiece's surfaces, (2) generating a sequence to visit all viewpoints in a time and kinematically optimal way, and (3) planning a feasible path to travel to each viewpoint. Additional criteria can be defined while planning the coverage path, including full coverage of the target surfaces and the resulting cycle-time for the inspection task (Glorieux et al., 2020). The existing CPP methods can be divided into two coarse categories: two-dimensional and three-dimensional methods.

Various researchers reported two-dimensional (2D) CPP for mobile robots in floor cleaning, bridge crack monitoring, and weed mowing tasks (Almadhoun et al., 2016; Galceran & Carreras, 2013). Veerajagadheswar et al. (2020) developed a motion planner for floor cleaning. Polyomino tiling theory was adapted to define reference coordinates and generate a navigation path to maximize the area coverage; Real-time experiments in different scenarios tested the planner on a Tetris-inspired shape-shifting robot. Hung M. La et al. (2013) proposed an autonomous robotic system for precise and efficient bridge deck inspection and identification, where a boustrophedon decomposition was applied to solve the CPP problem. Lim et al. (2014) developed an automatic detection and mapping system for automatic bridge crack inspection and

maintenance; They used an improved genetic algorithm to search for a CPP solution to minimize the number of turns and detection time while achieving an efficient bridge inspection. Danial Pour Arab et al. (2023) presented a CPP algorithm providing the optimal movements over an agricultural field; First, tree exploration was applied to find all potential solutions meeting predefined requirements, and then, a similarity comparison was proposed to find the best solution for minimizing overlaps, path length, and overall travel time.

It must be remarked that 2D CPP methods cannot be adopted directly for a three-dimensional (3D) CPP problem, as the level of complexity in 3D space is much higher than in 2D space. In most 2D applications, a complete planner map is available during planning. Most 3D CPP methods have to plan the paths from partial or occluded 3D maps. A CPP method for 3D reconstruction based on Building information modeling used a robot arm and a lifting mechanism for wall painting at construction sites (Zhou et al., 2022). It consists of a two-stage coverage planning framework, a global planner that can optimally generate the waypoints sequence, and a local planner that can provide the mobile base pose. The authors reported that this method could ensure coverage of all waypoints and improve painting efficiency. Hassan and Liu (2020) proposed an adaptive path planning approach capable of updating the paths when unexpected changes occur and still can attain the coverage goal. Zbiss. K et al. (2022) reported a path-planning method for collaborative robotic car painting. This proposed algorithm depends on computational geometry and convex optimization, and Morse cellular decomposition and boustrophedon algorithms are applied for path planning to generate a feasible and collision-free trajectory. A CPP method is based on Unmanned Aerial Vehicles (UAV) equipped LiDAR for bridge inspection (Bolourian & Hammad, 2020). This method combined a genetic algorithm and an A* algorithm to find a barrier-free and shortest path. This method planned the near-optimal and feasible path.

Recent studies on 3D CPP for industrial product quality detection focused on achieving full surface coverage of the workpiece with minimum inspection time are: Li et al. (2018) demonstrated a robust CPP method for aerospace structures based on their geometric features. Path planning relied on the feature graph construction through Voronoi Diagram. Then, a search method is proposed to find this graph to decide the inspection sequence and a convex hull-based approach is applied to avoid collisions. Glorieux et al. (2020) presented a targetted waypoint sampling strategy with the shortest inspection time for dimensional quality inspection of sheet metal parts. Liu et al. (2022) developed an enhanced rapidly exploring random tree (RRT*) method and integrated the inspection errors and the optimal number of viewpoints into measurement cost evaluation for higher precision in quality inspection. Huo et al. (2022) applied the nearest neighbor search algorithm to find a near-shortest scanning path aiming at convex free-form specular surface inspection.

Despite numerous recent developments, CPP for free-form surface inspection remains an open research problem. There are very few CPP solutions for line scanning robotic systems (Kapetanovic et al., 2018). Compared with area-scan sensors, a line-scanning sensor is more suitable for defect inspection in industrial/manufacturing applications due to higher spatial resolution and lower production costs (Steger &

Ulrich, 2021; Wang et al., 2022). Unlike a common area camera or other optical sensors that only work at some discrete positions, a line scanner utilizes only single beam scanning light to detect 3D objects when capturing images, and it needs to move continuously using a robotics manipulator along the coverage path. These features lead to many traditional CPP methods being ineffective. Therefore, developing a novel CPP method for the automatic line scanning system becomes imperative and advantageous.

This paper aims to overcome the limitations of existing CPP methods for surface defect inspection. We focus on defect detection for free-form surfaces of 3C workpieces based on a robotic line scanning system. This robotic system utilizes a 6-DOF robot manipulator with a line scanner to finish a full-coverage inspection path and a depth sensor to localize the workpiece. The proposed CPP method for robotics line scanning inspection consists of two parts, local path definition for accurate defect inspection and global time optimization for minimum scanning path. It incorporates the detailed requirements of 3C components surface inspection and the specific characteristics of a robotic line scanning system. The main contribution of this paper includes:

- (1) A new region segmentation method and an adaptive region-of-interest (ROI) algorithm to define the local scanning paths for free-form surfaces.
- (2) A Particle Swarm Optimization (PSO)-based global inspection path generation method to minimize the inspection time.
- (3) Detailed simulations, experiments, and comparisons to validate the proposed method.

The rest of this article is organized as follows. Section “[Coverage path planning for inspection](#)” describes the path planning problem for 3C component surface detection. Section “[Methodology](#)” presented the proposed CPP approach in detail. Section “[Case study](#)” shows the specific simulations, experiments, and comparisons on 3C components to validate the method’s feasibility. Finally, Section “[Conclusion](#)” concludes this article and discusses the limitations and future direction.

2 Coverage path planning for inspection

The CPP problem can be divided into two subproblems: 1) the local path definition is to generate view regions and partial scanning paths to meet the precise scanning and full coverage for 3C free-form workpieces. 2) global path planning aims to find an optimal or near-optimal sequence of all local paths (Gerbino et al., 2016).

The key to the first sub-problem determines the position and orientation of each pair of viewpoints at both ends of local paths (the path between two consecutive viewpoints). The line-scan camera only captures an image line of pixels at a time, so the relative motion perpendicular to the line of pixels between the camera and object is necessary for 2D image acquisition during the defect inspection task (see Fig. 1). In this automatic scanning system, the camera is moved with a robotics manipulator along the stationary object, and the direction of depth of view (DOV) of the camera should be perpendicular to the scanned region to ensure image quality. Therefore, the scanned area needs to keep as flat as possible even if models of workpieces include many different geometric features (see Fig. 2). In addition, each local path consists of two viewpoints at both ends of it, and the camera at the robotic end-effector could scan one

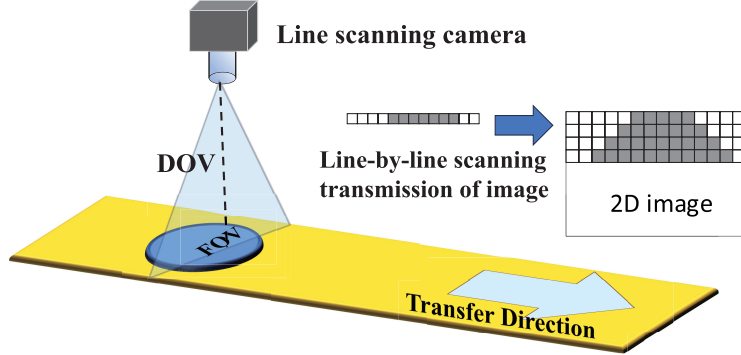


Fig. 1 Conceptual representation of line scanning sensor

viewpoint to another to inspect the surface defects of the regions corresponding to this local path. The change in the position of these two waypoints is required to be along one regular direction, whose orientations need to remain as unchanged as possible to ensure the quality of acquired images. Besides, this sub-problem is also affected by some critical factors, such as field of view (FOV) and DOV (Liu et al., 2022).

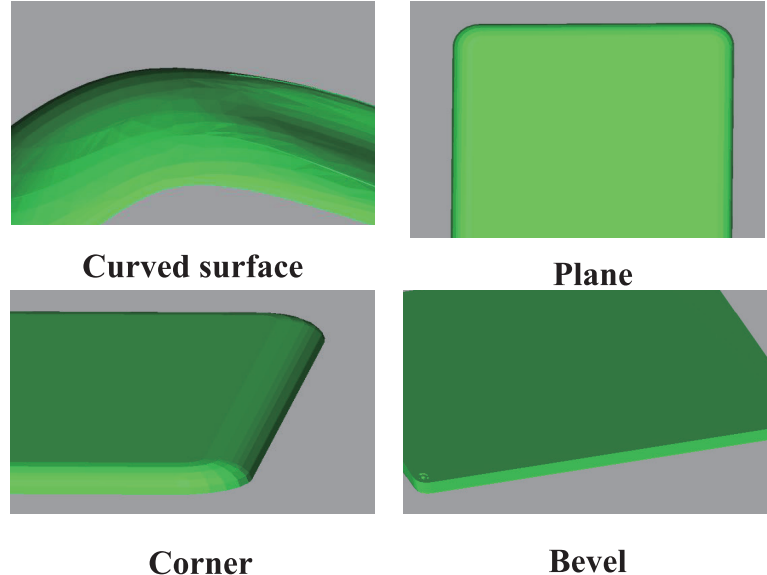


Fig. 2 Geometric features of 3C workpieces

The global path planning problem is concerned with finding the sequence and path connecting the selected viewpoints to minimize the total travel cost. This generated coverage path needs to reach all local paths with the shortest connection path. In other words, the objective is to find the minimum kinematic feasible path for the

robot manipulator to target the scanning sensor at each viewpoint precisely through all local paths, without colliding with any obstacles in the workspace.

This proposed method should provide a feasible coverage path that transverses all the local paths with minimum inspection time efficiently and automatically. Moreover, it needs to consider diverse measurement directions of local paths to ensure high detection precision. Generally, there are many local paths to evaluate the surface quality of the 3C components. To obtain precise defect original images, every scanning parameter is significant and could be set according to one new automatic method rather than the workers' experience and opinion.

3 Methodology

A CPP generation and optimization approach is presented based on the robotics line scanning system(see Fig. 3). This includes i) a new hybrid region segmentation method based on the random sample consensus (RANSAC) and K-means clustering method; ii) an adaptive ROI method to define the local measurement paths; and iii) one PSO-based global optimization approach for the minimum inspection time. This optimal path is then implemented for offline programming and surface detection, thereby improving the efficiency of the inspection of 3C components.

To exact the workpiece's geometry features, the 3D model is converted to a point cloud. The sampling procedure is based on selecting a series of points randomly and uniformly from the model to form a point cloud that can be used to segment and process all surfaces of the workpiece. The acquired point cloud O consists of points $p_i = [x_i, y_i, z_i], i = 1, 2, \dots, m$ (m is the total sampling number of O), which preserves the geometric information of all faces.

3.1 Hybrid region segmentation based on RANSAC and K-means clustering

The image acquisition characteristics of line-scan cameras necessitate the preservation of flat scanning areas to ensure optimal image quality. Therefore, it becomes crucial to employ an effective segmentation method to divide the entire surface into flat regions. In this study, we propose a hybrid region segmentation method specifically designed for the surface features of 3C components. This method leverages the RANSAC method and enhanced K-means clustering to achieve accurate segmentation. The RANSAC method is used to detect a region with planar geometry. It can also remove some points with minimum curvature from the entire point cloud, enhancing the computation speed of the whole procedure (Su et al., 2022). Furthermore, it can effectively remove outliers, thereby improving the accuracy of the subsequent K-means clustering process.

Here, we use RANSAC to partition O first. It includes two steps: producing an assumption by random samples and proving this assumption with the remaining data. Given different hypothesis geometrical models, RANSAC can identify planes, spheres, cylinders, and cones (Xu et al., 2016). Since the flat regions are required for precise line scanning, RANSAC utilized the equation of a plane as a feature model in the proposed system. It selects N sample points of O and estimates the plane model parameters by those sample points. The position of a point is selected as an inlier if

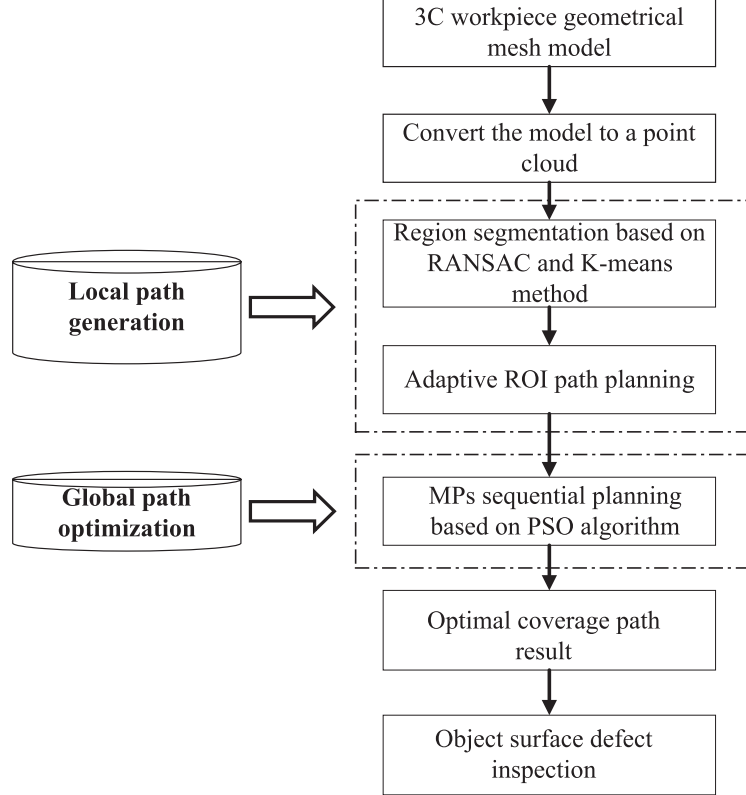


Fig. 3 Framework of the proposed method

the distance between the point and plane is less than the fixed thresholds and the shape that contains the greatest number of outlier points could be split and extracted after multiple iterations. The plane model can be represented as

$$aX + bY + cZ + d = 0 \quad (1)$$

where $[a, b, c, d]^T$ is the plane model parameter, and $[X, Y, Z]^T$ denotes any point in the 3D coordinates.

This method can extract a nearly planar point cloud region C_0 when the best plane model has been identified. RANSAC does not require complex optimization or high memory resource so that we can obtain C_0 rapidly. However, the remaining point cloud O^r with the size η^r cannot be segmented clearly by this approach since O^r consists of bevels, curved surfaces, and other complex geometrical information.

The traditional K-means clustering methods regarded the region segmentation as a clustering analysis problem of surface geometric features. They applied the position and surface normals of the point cloud for segmentation, which are not appropriate for workpieces with large variations in curvature or many bevels and corners (Li et

al., 2018; Liu et al., 2020). Therefore, Some different factors should be considered to describe the features of the object. The enhanced K-means clustering is proposed in this paper to process O^r . In the standard K-means method, the number of clusters N dramatically affects the performance of this method, and many trials are required to find a near-optimal N in some classical methods (Juang & Wu, 2011). In this developed method, we apply not only the corresponding surface normals $n_i^r = [n_{ix}^r, n_{iy}^r, n_{iz}^r]$ of the points in O^r but also the Gaussian curvature K_i^r and Mean curvature H_i^r of each point p_i^r in O^r as the inputs of the enhance K-means clustering. Besides, a feasible weighting factor ω among n_i^r , K_i^r , and H_i^r is determined through many manual experiments. K_i^r is the product of the principal curvatures of p_i^r , and it neutralizes the maximum and minimum curvatures. A positive Gaussian curvature value means the surface is locally either a summit or a valley, while a negative value illustrates the surface locally consists of saddle points. And zero Gaussian curvature indicates the surface is flat in at least one direction like a plane or cylinder (Li et al., 2019). In mathematics, the mean curvature of a surface presents the curvature of an inset surface in Euclidean space or other ambient spaces. The curvature of the point can be represented by $c_i^r = [K_i^r, H_i^r]$. With adding these two parameters in this enhanced K-means method, the clustering quality can be improved than before, so the geometric feature of the point of O^r is presented as $I_i^r = [n_i^r, c_i^r]$. Besides, we present a method to automatically adjust N since N affects the result of the classification, and the traditional techniques set one fixed N , whose drawback is its poor flexibility. The algorithm depends on a two-looped 1D search, with the inner loop for similarity comparison and the outer loop for iterating N . The iteration can end when the largest intra-class difference is smaller than a threshold T . The entire procedure of this enhanced K-means method is illustrated in Algorithm 1.

For the outer loop, we represent the feature vectors of the N -cluster set as

$$Q_j = [q_n, q_c] \quad q_n = [q_1, q_2, q_3] \quad q_c = [q_4, q_5] \quad (2)$$

Q_j is one 5-dimensional vector ($j = 1, 2, \dots, N$). All of them can be initialized with a random value. Afterward, the procedure goes into the inner loop, composed of two steps: 1) similarity comparison and 2) updating. In the first step, cosine similarity is used in this proposed method for assessing the similarity between I_i^r and Q_j , which is considered as a measure of similarity between two sequences of numbers in data analysis (Kiricsi et al., 2023). The similarity α_{ij} is described in detail as follows:

$$\alpha_{ij} = \omega_1 \cos \left(\frac{n_i^r \cdot q_n}{|n_i^r| \cdot |q_n|} \right) + \omega_2 \cos \left(\frac{c_i^r \cdot q_c}{|c_i^r| \cdot |q_c|} \right) \quad (3)$$

where ω_1 and ω_2 are the weighting factors for α_{ij} , and they are set as 0.6 and 0.4 respectively in this method according to many experiments.

Then, this method should find the cluster C_j with the smallest α_{ij} and exact the corresponding p_i^r and I_i^r to it. The next step is to determine whether the classification has met the termination condition. For each cluster C_j , the termination parameter λ_j

is calculated from the maximum intra-class difference D_j as:

$$\lambda_j = \begin{cases} 0, & D_j > T \\ 1, & \text{else} \end{cases} ; D_j = \max_i \alpha_{ij} \quad (4)$$

β_t represents the sum of λ_j from every region C_j at this iteration t . If $\beta_t = N$, the current segmentation is satisfactory and the algorithm can finish iteration. Otherwise, the procedure continues. In this stage, the search direction should be considered since the method includes two loops, the inner one that compares similarity and clusters concerning N and the outer one that increases the value of N gradually. The change relies on the performance of β_t . If the performance deteriorates at the iteration step t (i.e. β_t is smaller than β_{t-1}), the inner loop must stop immediately and a new outer loop starts with $N \leftarrow N + 1$ because the current N is not ideal. If the performance is better (i.e. β_t is larger than β_{t-1}), the search within the inner loop continues.

Before switching to the next inner iteration, all feature vector $Q_j = [q_n, q_c]$ are updated to improve the representation level:

$$q_n = \frac{\frac{1}{\eta_j} \sum_{i=1}^{\eta_j} n_{ij}}{\left\| \frac{1}{\eta_j} \sum_{i=1}^{\eta_j} n_{ij} \right\|} \quad q_c = \frac{\frac{1}{\eta_j} \sum_{i=1}^{\eta_j} c_{ij}}{\left\| \frac{1}{\eta_j} \sum_{i=1}^{\eta_j} c_{ij} \right\|} \quad (5)$$

where n_{ij} , c_{ij} and η_j are i -th normal feature vector in C_j , curvature feature vector in C_j and the size of the C_j separately.

The proposed algorithm only takes the limited features of the region C_j into consideration, which can lead to a high sparsity of the clustered points within the same region. Therefore, Euclidean cluster extraction is implemented as a post-processing step to verify if it is necessary to subdivide the region C_j into two new regions according to the location of the points in it.

Algorithm 1 The enhanced K-means Region Segmentation

Require: T, O_r
Ensure: $C_j, j = 1, 2, \dots, N$

- 1: **while** $\beta_t < N$ **do**
- 2: Initialize Q_j ; randomly, $j = 1, 2, \dots, N$;
- 3: **while** $\beta_t \geq \beta_{t-1}$ **do**
- 4: **for** $i = 1 : \eta^r$ **do**
- 5: Compute similarity $\alpha_{ij} \leftarrow (3)$;
- 6: $j_{\text{argmin}} \leftarrow \text{argmin } \alpha_{ij}$, take $p_i^r \rightarrow C_j$;
- 7: **end for**
- 8: Calculate: $\beta_t \leftarrow (4)$;
- 9: Update: $Q_j \leftarrow (5)$;
- 10: **end while**
- 11: $N \leftarrow N + 1$;
- 12: **end while**

3.2 Adaptive ROI Based Path Planning

The local paths are generated according to the proposed planning method, which takes the segmented region C_j as input. Due to the synchronization of the scanning inspection of the line camera and the robot's motion, every viewpoint in these local paths should be produced through a feasible method for accurate detection, and all local paths are required to cover the whole region C_j of the workpiece. Hence, this part presents an adaptive ROI method for generating local paths that aim to adapt scan paths and viewpoints to the various shapes of objects

Since the scanning sensor captures a horizontal line image, the scanning coverage can be thought of as a cuboid when the system is moving linearly, which contains the DOV V_D , the FOV V_F , and the moving direction V_L (see Fig. 4). Besides, the key of this approach is to determine the position $\mu = [x, y, z]$ and pose $i = [\vec{d}, \vec{l}]$ of the viewpoints (v^p, v^{p*}) at both ends of a local path $G_t, t = 1, 2, \dots, U$. The pose i is described by the direction \vec{d} of V_D and the direction \vec{l} of V_L .

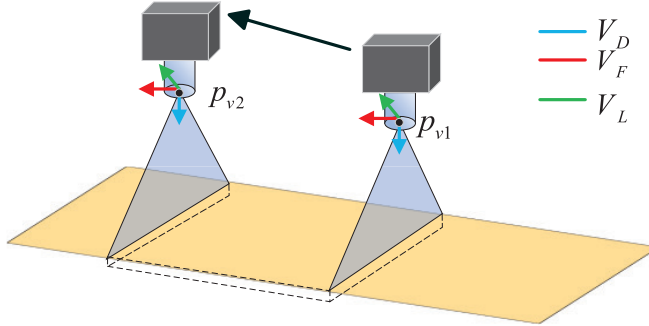


Fig. 4 Cuboid coverage generation of line scanning camera during linear motion

To make the geometric scanning model effective and keep the accuracy of this system, our algorithm further segments every C_j into 3 sub-regions $W_{jf}, f = 1, 2, 3$. Due to the irregular shape of each C_j , we stipulate that the C_j is divided into 3 sub-region W_{jf} evenly following the direction \vec{k} of the longest length of each C_j and the scanning motion is also along \vec{k} for every area ($\vec{l} = \vec{k}$). In addition, we define that \vec{d} is the reverse direction of the surface normal \vec{w}_{jf} of this W_{jf} ($\vec{d} = -\vec{w}_{jf}$).

Thus, the corresponding μ_1, μ_2 are located on :

$$\mu = \tau - \vec{w}_{jf} \cdot |V_D| \quad (6)$$

The center of the sub-region W_{jf} is regarded as $c_{jf} = [c_x, c_y, c_z]$, and the intersections τ_1, τ_2 of the W_{jf} 's edge and the line $\vec{k} \cdot c_{jf}$ are deemed as the inspection points of viewpoints v^p, v^{p*} at both ends of a local path G_t on this sub-region surface. $|V_D|$ is the magnitude of V_D .

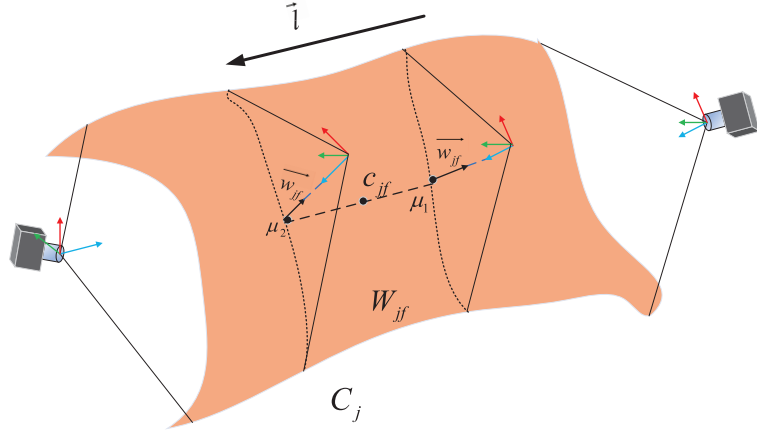


Fig. 5 Further region segmentation and linear path planning

3.3 PSO-based global path optimization

Based on the local path definition in the previous step, we need to find an optimal sequence of all local paths to generate a complete scanning path for the whole free-form workpiece surface. We should consider how to minimize the total robot's motion time under a constant velocity of the sensor during the inspection task. According to the requirements in practice, the robotics manipulator should complete the scanning inspection task through all pre-defined viewpoints. This sequence optimization problem can be regarded as Traveling Salesman Problem (TSP) to obtain a path with the shortest time (Claro et al., 2023). The TSP is one integrated optimization problem and nondeterministic polynomial time (NP)-hard. The problem of global path planning can be formulated

$$\min \left\{ \sum_{t=1}^U \sum_{s=1}^{U-1} T_t^{scanning} + T_s^{across} \right\} \quad (7)$$

where $T_t^{scanning}$ is the cost time of passing every local path G_t , T_s^{across} means the cost time from G_t to G_{t+1} and U represents the total number of local paths. The cost time in the context of the robot manipulator's end-effector is determined by the straight-line distance between two viewpoints, considering the constant speed of movement. In contrast to the general TSP, our scenario requires sequential traversal of adjacent viewpoints within the same local path to ensure optimal inspection performance. This constraint is imposed due to the limitations of region segmentation and the necessity for adaptive ROI local path definition. The limitation can be summarized as

$$T_t^{scanning}(G_t) = \begin{cases} T(v_t^p \rightarrow v_t^{p*}) \\ T(v_t^{p*} \rightarrow v_t^p) \end{cases} \quad (8)$$

$$T_s^a cross(G_t, G_{t+1}) = \begin{cases} T(v_t^p \rightarrow v_{t+1}^p) \\ T(v_t^p \rightarrow v_{t+1}^{p*}) \\ T(v_t^{p*} \rightarrow v_{t+1}^{p*}) \\ T(v_t^{p*} \rightarrow v_{t+1}^p) \end{cases} \quad (9)$$

The prior studies on this problem include branch and bound linear programming, and dynamic programming methods (Shang et al., 2020; Xu et al., 2023). However, with the increasing number of targets, the computation of a feasible path becomes exponentially more difficult, and obtaining the global optimal solution becomes more challenging. Different heuristic algorithms have been developed for TSP, including Simulated Annealing, Genetic Algorithm, Ant Colony Optimization, A* algorithm, etc (Abualigah & Diabat, 2023); Ghali et al., 2023). In the proposed method, the PSO-based method is used to solve TSP with the advantage of general flexibility in TSP solving. After selecting the shortest path, the optimal general path sequence can be acquired in this step. In PSO (Karim et al., 2021), a swarm of particles are used to describe the possible solutions. Every particle ξ is related to two vectors in D -dimension space, i.e., the velocity vector $\mathbf{V}_\xi = [V_\xi^1, V_\xi^2, \dots, V_\xi^D]$ and the position vector $\mathbf{X}_\xi = [X_\xi^1, X_\xi^2, \dots, X_\xi^D]$. Both of them are initialized by random vectors. During the PSO process, the velocity and position of particle ξ on dimension d are updated as (Zhan et al., 2009):

$$V_\xi^d = \omega V_\xi^d + c_1 \text{rand}_1^d (pBest_\xi - X_\xi^d) + c_2 \text{rand}_2^d (gBest - X_\xi^d) \quad (10)$$

$$X_\xi^d = X_\xi^d + V_\xi^d \quad (11)$$

where ω represents the inertia weight, and c_1 and c_2 are random numbers within $[0,1]$. $pBest_\xi$ is the position with the best fitness value for the ξ th particle and $gBest$ is the best position in the global. The main steps of PSO are:

- (1) Initialize all particles, including their velocity and position.
- (2) Establish the fitness function and calculate the fitness value of each particle,
- (3) Update the $pBest_\xi$ and $gBest$.
- (4) Update the velocity and position of each particle according to (10) and (11).
- (5) Increase the number of iterations, Go to step 3 and repeat until the termination condition.

4 Case study

To illustrate the performance of the proposed method, we provide two case studies for simulation tests (Case 1: a camera lens, Case 2: a Computer fan) and two case studies for experimental evaluation (Case 3: a tablet back cover, Case 4: upper part of computer mouse) on 3C component surface inspection. A state-of-the-art CPP method is also used for comparison with the developed method in “Comparative analysis and verification”.

4.1 Case study setup

Fig. 6 shows the experimental setup for evaluating the proposed methods. A custom-made end-effector housed the defect inspection system consisting of a line scanning sensor (Hikvision MV-CL041-70GM camera) and a uniform line illumination source (TSD-LSH230200-B from TSD company). The Intel RealSense L515 LiDAR camera was mounted on the top of the workspace to capture the real-time stream of point clouds. The pose of the workpiece was estimated using the point clouds from LiDAR. An analog control box with a high-power strobe ensures an adjustable and stable voltage for the light source. The system consisted of a UR5 manipulator from Universal Robots to manipulate the end-effector in order to scan the workpiece automatically. The entire automated line scanning framework is based on ROSon Linux PC, which can simultaneously monitor the sensors (line scanner, depth sensor) and control the actuator (manipulator).

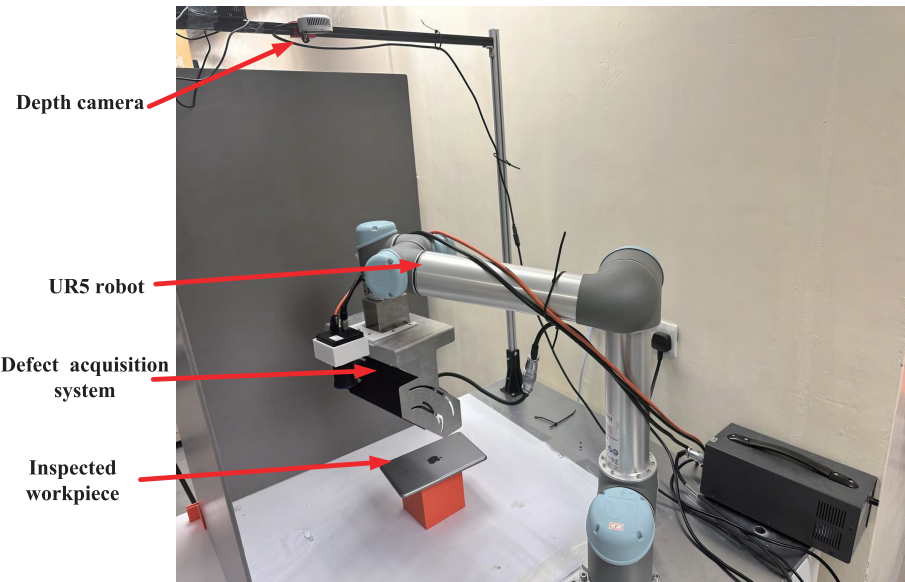


Fig. 6 Experimental setup of the automated line scanning system

Table 1 The parameters used in the case study

Parameter	Value
V_D (mm)	300
V_F (mm)	70
Sampling frequency(Hz)	10000
Image resolution	3000*680

The line velocity and acceleration of the manipulator's end-effector were empirically set to 0.05 m/s and 0.5 m/s^2 , respectively. During trajectory execution, the robot manipulator followed a constant line speed to maintain consistency of image acquisition (the acquisition line rate of the scanner is 3000 line/s). Table 1 summarizes the other parameters for the line scanning system used for the experiment.

4.2 Path generation and defect inspection

Fig. 7 presents four 3C component models. Each 3D mesh model (or CAD model) was converted into a point cloud to identify the geometrical features through uniform and random sampling (Arias-Castro et al., 2006), as shown in Fig. 7. Some geometrical features, such as surface normals, Gaussian curvature, and mean curvature, are computed by a point cloud processing software named CloudCompare (Tang et al., 2023). Then, the point cloud was inputted into the proposed method for estimating the scanning path. The similarity threshold T should be selected before region segmentation. If T is large, the segmentation process needs more computation time to cluster the point cloud, which could reduce the overall clustering efficiency. On the contrary, a smaller value of T groups the different features into the same cluster C_j , which degrades the segmentation accuracy. Consequently, selecting this component must balance the segmentation accuracy and calculation efficiency. 0.64 is an optimal value for T , found by hit and trials.

The results from the hybrid segmentation method are shown in Fig. 8, where the different colors indicate various segmented regions (or clusters). Here, the methods used RANSAC to cluster the plane region. In Case 3 and Case 4, a significant portion of the planar/near-planar region has been grouped in one cluster, as shown in Fig. 8(c). Initial clustering using RANSAC significantly reduces the processing time. After the hybrid unsupervised region segmentation, the surfaces with similar geometric features were clustered together. Fig. 8 shows the four geometrically diverse workpieces, and each is divided into different regions based on the features. Some segmentation errors will remain due to the uncertain nature of computing features, but if they do not affect the scanning path generation.

With adaptive ROI-based path planning and PSO-based global path generation, a complete and near-optimal inspection path can be produced, which is visualized in Fig. 9. The number of viewpoints is 48, 48, 42, and 30 in Case 1-4 respectively, displayed by the frames. They show the pose of the robot's end-effector during the inspection task. The global path planning is demoted with a black line and every segmentated region has a corresponding local path. The different viewpoints are connected by straight lines in the optimal sequence. The robotics motion should follow this detection path to achieve full object coverage.

We input the inspection paths to the automatic line scanning system to scan the tablet back cover and upper part of computer mouse in order to mimic the real defect inspection, as illustrated in Fig. 10. Fig. 11 illustrates the surface defects of these two objects. Since the segmented results have similar geometric features, and the feasible viewpoints can be selected by the ROI-based method based on the parameters of the line-scan camera, surface defects can be acquired clearly, even where the defects are easy to ignore for a human eye, like corners and curved surfaces. The proposed method

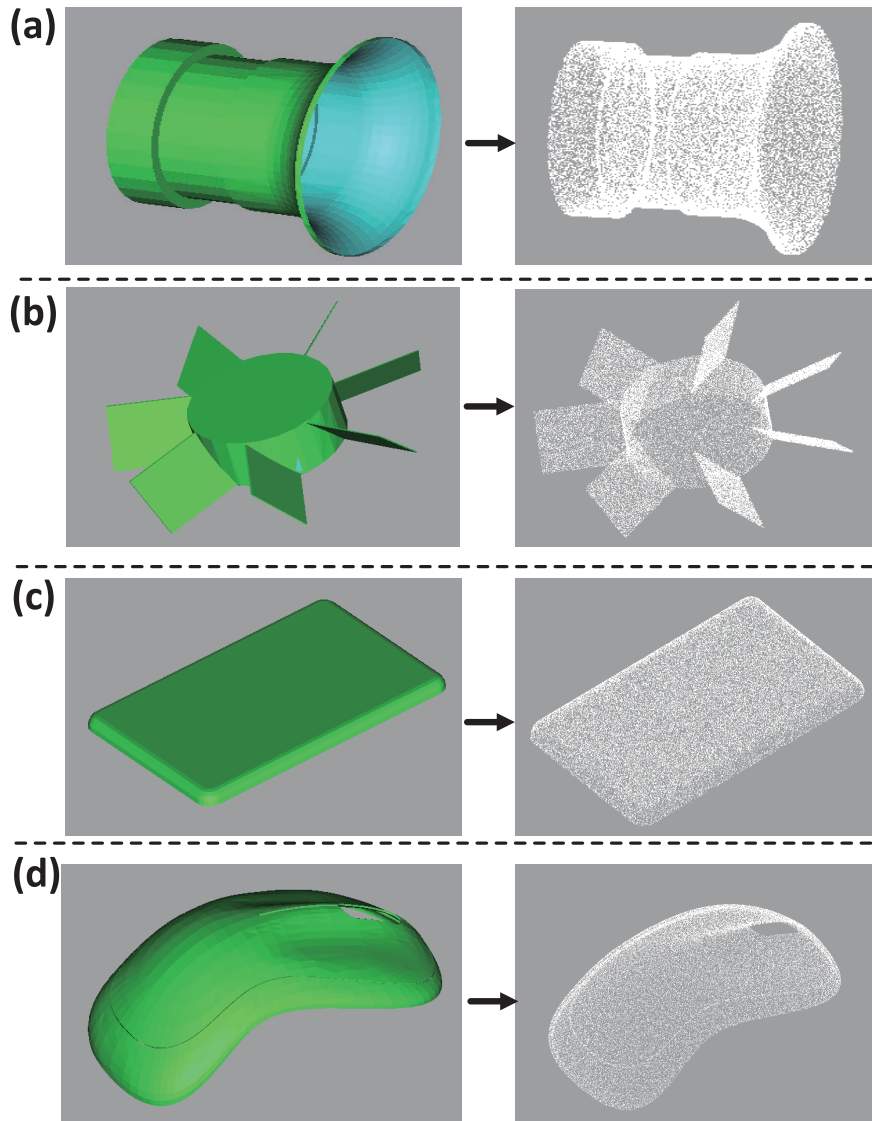


Fig. 7 The model and point cloud of workpieces, (a) Case 1: the camera lens; (b) Case 2: the computer fan; (c) Case 3: the tablet back cover; (d) Case 4: upper part of computer mouse

can effectively conduct region segmentation, local path planning, and global path optimization, enabling precise surface defect inspection and further process optimization for the 3C industry.

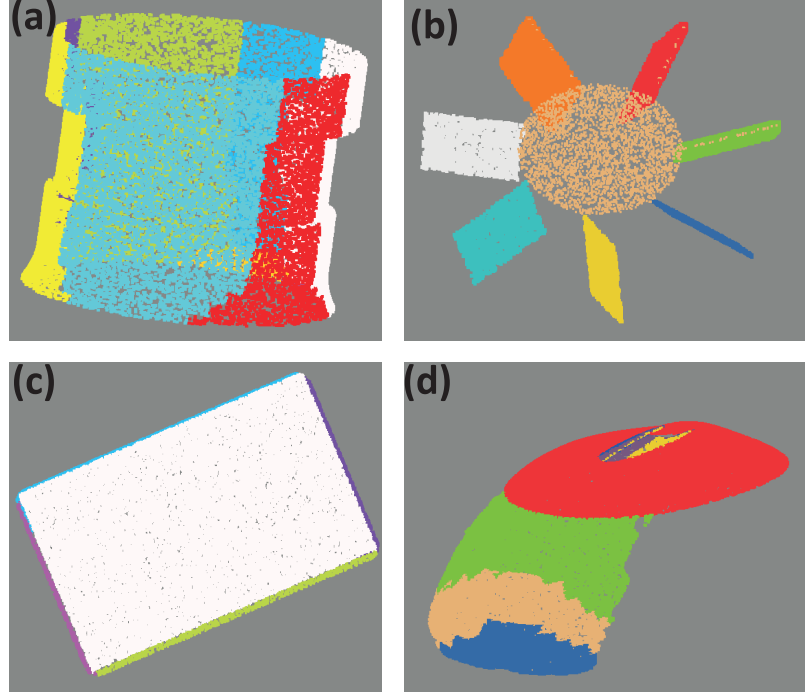


Fig. 8 The segmentation result by the proposed method, (a) Case 1: the camera lens; (b) Case 2: the computer fan; (c) Case 3: the tablet back cover; (d) Case 4: upper part of computer mouse

4.3 Comparative analysis and verification

To further validate the proposed CPP method, a cutting-edge line scanning CPP method (Hu et al., 2022), a convex specular surface inspection method, is applied as a benchmark approach for comparative analysis. In this method, the traditional K-means clustering method is used for region segmentation and they produced the final path through a local optimization method, nearest neighbor search (Aryal et al., 1998).

There are five comparison criteria: region segmentation time, total number of viewpoints, length of the global inspection path, total inspection time, and surface defect detection rate. Segmentation time was used as a measure of efficiency for region segmentation methods. The inspection path length and total detection time served as indicators of overall path efficiency in CPP methods. The surface defect detection rate provided insights into the actual effectiveness of defect acquisition, reflecting the accuracy of region segmentation and the quality of path planning. Additionally, when defect results or coverage rates were similar, preference was given to the CPP method that generated fewer viewpoints as it was considered a more viable path planning approach (Liu et al., 2020).

The comparison results are shown in Fig. 12. For region segmentation time, the proposed time used less time to finish this procedure. Due to the usage of RANSAC and more geometric features, the proposed method can obtain the subregions with planar/near-planar geometry efficiently. As for the viewpoints, our developed approach

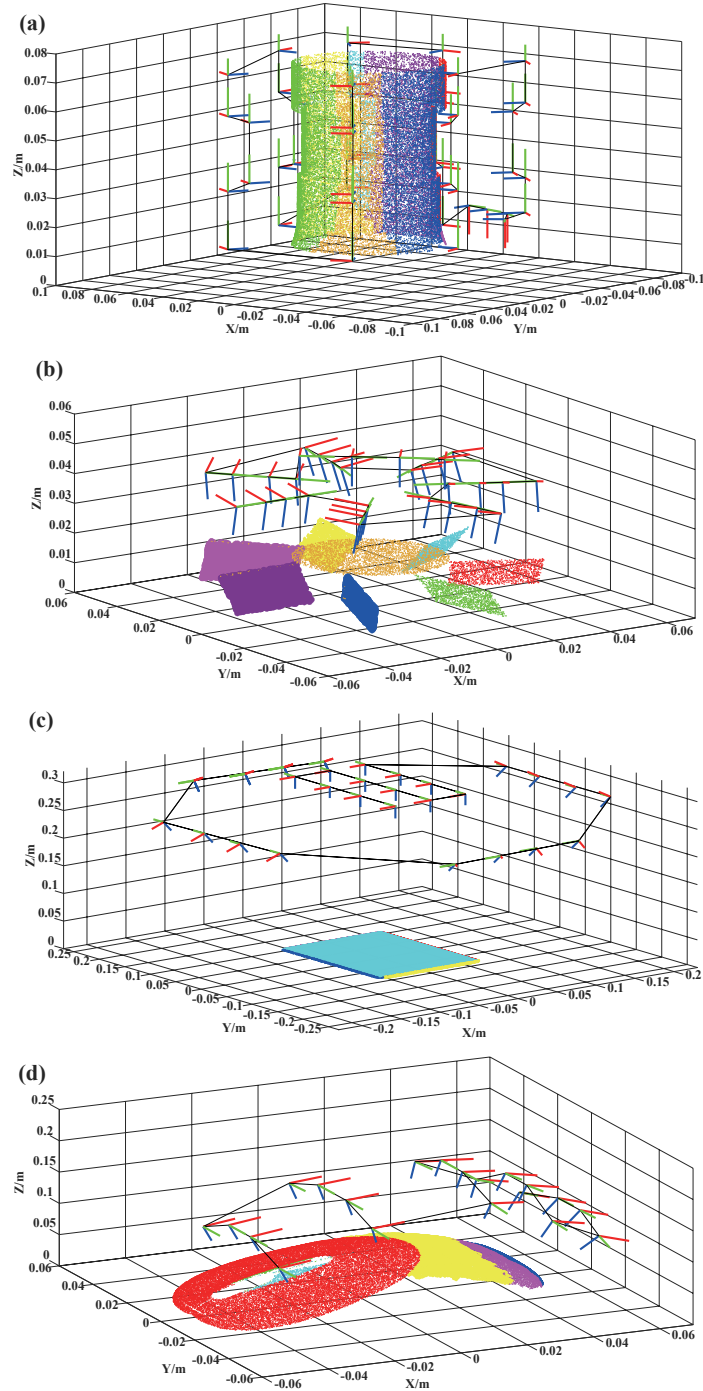


Fig. 9 Coverage path planning through the proposed method, (a) Case 1: the camera lens; (b) Case 2: the computer fan; (c) Case 3: the tablet back cover; (d) Case 4: upper part of computer mouse

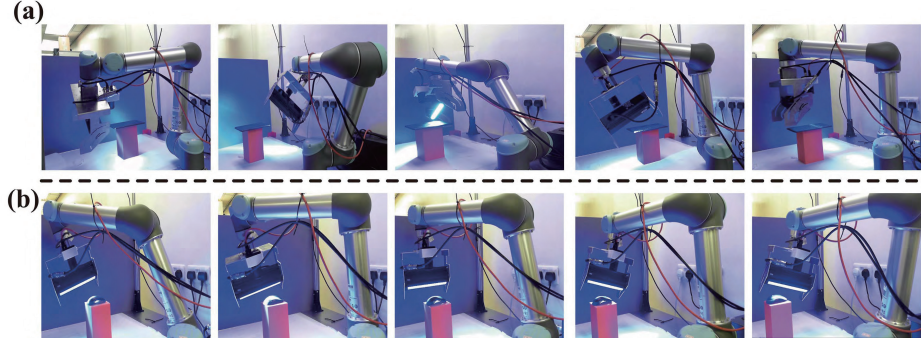


Fig. 10 Experimental scenarios of 3C component surface inspection by the proposed method, (a) Case 3: the tablet back cover; (b) Case 4: upper part of computer mouse

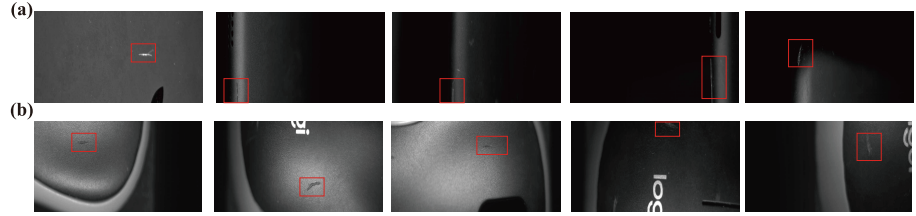


Fig. 11 Representative defect images obtained by the proposed method, (a) Case 3: the tablet back cover; (b) Case 4: upper part of computer mouse

produces fewer viewpoints since more accurate region segmentation results and concise ROI generation. Conversely, the convex specular surface inspection method employed a more complex iteration process for viewpoint determination, as it struggled to precisely segment objects with intricate geometries. When comparing inspection path length and time, our method outperformed the benchmark approach. While the benchmark utilized a local optimization solution, namely nearest neighbor search, it fell short in generating a feasible global inspection path for CPP. In contrast, our PSO-based method effectively addressed the TSP with reasonable optimization goals and feasible viewpoints. Although our approach is slightly better than its surface defect detection rate, the presented method can finish the inspection task with less time and shorter paths. Based on this comprehensive comparison, our proposed CPP method stands as a superior choice over the state-of-the-art line scanning inspection method. Consequently, the proposed method presents a valuable and feasible solution for CPP in surface defect inspection.

5 Conclusion

This paper proposes a systematic framework for an inspection CPP method for 3C component surfaces. According to this framework, a high-resolution line scanning sensor, mounted on a multi-DOF robotic manipulator, can execute surface scanning and detection precisely and flexibly. The developed methodology includes (1) a new hybrid region segmentation method based on the RANSAC and K-means clustering method;

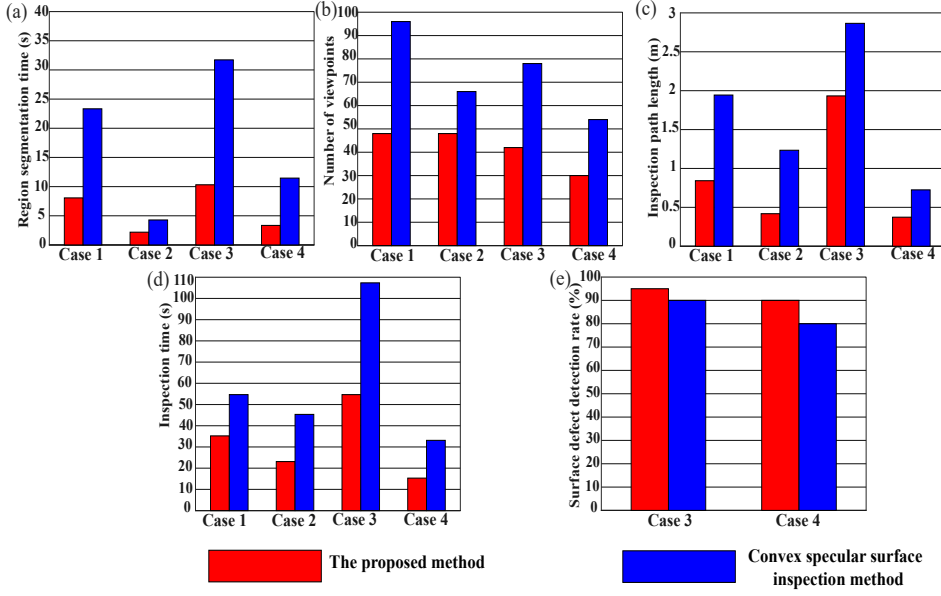


Fig. 12 Results of the proposed method and Convex specular surface inspection method in Case 1-4. Comparison of (a) Region segmentation time, (b) Number of viewpoints, (c) Inspection path length, (d) Inspection time, and (e) surface defect detection rate

(2) an adaptive ROI method to define the local measurement paths; and (3) a PSO-based global optimization approach for the minimum inspection time. Four case studies verify the effectiveness and efficiency of this method. The results show it outperforms the state-of-the-art line scanning CPP method according to comparison. Overall, the proposed method can achieve precise and efficient surface inspection for 3C free-from components. It can be applied in the 3C industry and be extended to inspect other structures such as auto spare parts and industry-standard components.

However, it should be noted that the proposed method may encounter challenges when applied to workpieces with complex structures, making it less suitable for parts with intricate shapes. Future research should focus on optimizing the design of the system end-effector to enhance the flexibility of the inspection framework. Additionally, exploring mathematical methods for optimal path planning and investigating the potential of information theory and deep learning techniques, such as convolutional neural networks, could further improve the effectiveness of the segmentation method.

Supplementary information The following video demonstrates the performance of the proposed method with simulations and experiments: <https://vimeo.com/842785212>.

Funding This work was supported by the grant from Shanghai Microintelligence Technology Co. Ltd (No. P21-0078).

Declarations

Competing interests The authors declare that they have no known competing financial interests or personal relationships that could have appeared to influence the work reported in this paper.

Data availability statement The data underlying this article will be shared on reasonable request to the corresponding author.

Authors' contribution **Hongpeng Chen**: Conceptualization, Methodology, Software, Validation, Writing – original draft. **Shengzeng Huo**: Software, Validation, Writing – review & editing. **Muhammad Muddassir**: Conceptualization, Validation, Writing – review & editing. **Hoi-Yin Lee**: Video Making, Validation, Writing – review & editing. **Anqing Duan**: Methodology, Data curation, Writing – review & editing. **Pai zheng**: Supervision, Resources, Conceptualization. **Hongsheng Pan**: Resources, Funding acquisition, Writing – review & editing. **David Navarro-Alarcon**: Supervision, Resources, Conceptualization, Methodology, Funding acquisition, Writing – review & editing.

References

Abualigah, L., & Diabat, A. (2023, APR). Improved multi-core arithmetic optimization algorithm-based ensemble mutation for multidisciplinary applications. *Journal of Intelligent Manufacturing*, 34(4), 1833-1874, <https://doi.org/10.1007/s10845-021-01877-x>

Almadhoun, R., Taha, T., Seneviratne, L., Dias, J., Cai, G. (2016, NOV 18). A survey on inspecting structures using robotic systems. *International Journal of Advanced Robotic Systems*, 13, , <https://doi.org/10.1177/1729881416663664>

Arab, D.P., Spisser, M., Essert, C. (2023, 2023 MAY 9). Complete coverage path planning for wheeled agricultural robots. *Journal of Field Robotics*, , <https://doi.org/10.1002/rob.22187>

Arias-Castro, E., Donoho, D.L., Huo, X. (2006, FEB). Adaptive multiscale detection of filamentary structures in a background of uniform random points. *ANNALS OF STATISTICS*, 34(1), 326-349, <https://doi.org/10.1214/009053605000000787>

Arya, S., Mount, D., Netanyahu, N., Silverman, R., Wu, A. (1998, NOV). An optimal algorithm for approximate nearest neighbor searching in fixed dimensions. *Journal of the ACM*, 45(6), 891-923, <https://doi.org/10.1145/293347.293348>

Bolourian, N., & Hammad, A. (2020, SEP). Lidar-equipped uav path planning considering potential locations of defects for bridge inspection. *Automation in Construction*, 117, , <https://doi.org/10.1016/j.autcon.2020.103250>

Chen, H., Xu, H., Yang, Z. (2022). A novel hybrid method to detect arrival times of elastic waves with low snr based on jensen-shannon divergence and cumulative sum algorithm. *IEEE Transactions on Instrumentation and Measurement*, 71, , <https://doi.org/10.1109/TIM.2022.3212529>

Chen, H., & Yang, Z. (2021). Arrival picking of acoustic emission signals using a hybrid algorithm based on aic and histogram distance. *IEEE Transactions on Instrumentation and Measurement*, 70, , <https://doi.org/10.1109/TIM.2020.3041103>

Claro, R.M., Pereira, M.I., Neves, F.S., Pinto, A.M. (2023). Energy efficient path planning for 3d aerial inspections. *IEEE Access*, 11, 32152-32166, <https://doi.org/10.1109/ACCESS.2023.3262837>

Galceran, E., & Carreras, M. (2013, DEC). A survey on coverage path planning for robotics. *Robotics and Autonomous Systems*, 61(12), 1258-1276, <https://doi.org/10.1016/j.robot.2013.09.004>

Gerbino, S., Del Giudice, D.M., Staiano, G., Lanzotti, A., Martorelli, M. (2016, JUN). On the influence of scanning factors on the laser scanner-based 3d inspection process. *The International Journal of Advanced Manufacturing Technology*, 84(9-12), 1787-1799, <https://doi.org/10.1007/s00170-015-7830-7>

Ghali, M., Elghali, S., Aifaoui, N. (2023, 2023 MAY 2). Genetic algorithm optimization based on manufacturing prediction for an efficient tolerance allocation approach. *Journal of Intelligent Manufacturing*, , <https://doi.org/10.1007/s10845-023-02132-1>

Glorieux, E., Franciosa, P., Ceglarek, D. (2020, FEB). Coverage path planning with targetted viewpoint sampling for robotic free-form surface inspection. *Robotics and Computer-Integrated Manufacturing*, 61, , <https://doi.org/10.1016/j.rcim.2019.101843>

Hassan, M., & Liu, D. (2020, FEB). Ppcpp: A predator-prey-based approach to adaptive coverage path planning. *IEEE Transactions on Robotics*, 36(1), 284-301, <https://doi.org/10.1109/TRO.2019.2946891>

Huo, S., Zhang, B., Muddassir, M., Chik, D.T.W., Navarro-Alarcon, D. (2022, FEB 1). A sensor-based robotic line scan system with adaptive roi for inspection of defects over convex free-form specular surfaces. *IEEE Sensors Journal*, 22(3), 2782-2792, <https://doi.org/10.1109/JSEN.2021.3132428>

Juang, L.-H., & Wu, M.-N. (2011, JUN). Psoriasis image identification using k-means clustering with morphological processing. *Measurement*, 44(5), 895-905, <https://doi.org/10.1016/j.measurement.2011.02.006>

Kapetanovic, N., Miskovic, N., Tahirovic, A., Bibuli, M., Caccia, M. (2018). A side-scan sonar data-driven coverage planning and tracking framework. *Annual Reviews in Control*, 46, 268-280, <https://doi.org/10.1016/j.arcontrol.2018.10.012>

Karim, A.A., Isa, N.A.M., Lim, W.H. (2021). Hovering swarm particle swarm optimization. *IEEE Access*, 9, 115719-115749, <https://doi.org/10.1109/ACCESS.2021.3106062>

Kirisci, M. (2023, FEB). New cosine similarity and distance measures for fermatean fuzzy sets and topsis approach. *Knowledge and Information Systems*, 65(2), 855-868, <https://doi.org/10.1007/s10115-022-01776-4>

La, H.M., Lim, R.S., Basily, B.B., Gucunski, N., Yi, J., Maher, A., ... Parvardeh, H. (2013, DEC). Mechatronic systems design for an autonomous robotic system for high-efficiency bridge deck inspection and evaluation. *IEEE/ASME Transactions on Mechatronics*, 18(6), 1655-1664, <https://doi.org/10.1109/TMECH.2013.2279751>

Li, B., Feng, P., Zeng, L., Xu, C., Zhang, J. (2018, DEC). Path planning method for on-machine inspection of aerospace structures based on adjacent feature graph. *Robotics and Computer-Integrated Manufacturing*, 54, 17-34, <https://doi.org/10.1016/j.rcim.2018.05.006>

Li, D., Cao, Y., Tang, X.-s., Yan, S., Cai, X. (2018, NOV). Leaf segmentation on dense plant point clouds with facet region growing. *Sensors*, 18(11), , <https://doi.org/10.3390/s18113333>

Li, P., Wang, R., Wang, Y., Gao, G. (2019, DEC). Automated method of extracting urban roads based on region growing from mobile laser scanning data. *Sensors*, 19(23), , <https://doi.org/10.3390/s19235262>

Li, Z., Tang, K., Hu, P., Huang, L. (2023, APR). Five-axis trochoidal sweep scanning path planning for free-form surface inspection. *IEEE Transactions on Automation Science and Engineering*, 20(2), 1139-1155, <https://doi.org/10.1109/TASE.2022.3179628>

Lim, R.S., La, H.M., Sheng, W. (2014, APR). A robotic crack inspection and mapping system for bridge deck maintenance. *IEEE Transactions on Automation Science and Engineering*, 11(2), 367-378, <https://doi.org/10.1109/TASE.2013.2294687>

Liu, M., Shao, Y., Li, R., Wang, Y., Sun, X., Wang, J., You, Y. (2020, MAY 29). Method for extraction of airborne lidar point cloud buildings based on segmentation. *Plos One*, 15(5), , <https://doi.org/10.1371/journal.pone.0232778>

Liu, Y., Zhao, W., Liu, H., Wang, Y., Yue, X. (2022, OCT). Coverage path planning for robotic quality inspection with control on measurement uncertainty. *IEEE/ASME Transactions on Mechatronics*, 27(5), 3482-3493, <https://doi.org/10.1109/TMECH.2022.3142756>

Liu, Y., Zhao, W., Lutz, T., Yue, X. (2022, DEC). Task allocation and coordinated motion planning for autonomous multi-robot optical inspection systems. *Journal of Intelligent Manufacturing*, 33(8), 2457-2470, <https://doi.org/10.1007/s10845-021-01803-1>

Liu, Y., Zhao, W., Sun, R., Yue, X. (2020, JUL). Optimal path planning for automated dimensional inspection of free-form surfaces. *Journal of Manufacturing Systems*, 56, 84-92, <https://doi.org/10.1016/j.jmsy.2020.05.008>

Luo, Q., & He, Y. (2016, APR). A cost-effective and automatic surface defect inspection system for hot-rolled flat steel. *Robotics and Computer-Integrated Manufacturing*, 38, 16-30, <https://doi.org/10.1016/j.rcim.2015.09.008>

Ming, W., Shen, F., Li, X., Zhang, Z., Du, J., Chen, Z., Cao, Y. (2020, JUL 1). A comprehensive review of defect detection in 3c glass components. *Measurement*, 158, , <https://doi.org/10.1016/j.measurement.2020.107722>

Molina, J., Ernesto Solanes, J., Arnal, L., Tornero, J. (2017, DEC). On the detection of defects on specular car body surfaces. *Robotics and Computer-Integrated Manufacturing*, 48, 263-278, <https://doi.org/10.1016/j.rcim.2017.04.009>

Shang, Z., Bradley, J., Shen, Z. (2020, NOV 15). A co-optimal coverage path planning method for aerial scanning of complex structures. *Expert Systems with Applications*, 158, , <https://doi.org/10.1016/j.eswa.2020.113535>

Steger, C., & Ulrich, M. (2021, JAN). A camera model for line-scan cameras with telecentric lenses. *International Journal of Computer Vision*, 129(1), , <https://doi.org/10.1007/s11263-020-01358-3>

Su, Z., Gao, Z., Zhou, G., Li, S., Song, L., Lu, X., Kang, N. (2022, JAN). Building plane segmentation based on point clouds. *Remote Sensing*, 14(1), , <https://doi.org/10.3390/rs14010095>

Tang, Y., Wang, Y., Tan, H., Peng, W., Xie, H., Liu, X. (2023). A digital twin-based intelligent robotic measurement system for freeform surface parts. *IEEE Transactions on Instrumentation and Measurement*, 72, 1-13, <https://doi.org/10.1109/TIM.2023.3261933>

Veerajagadheswar, P., Ping-Cheng, K., Elara, M.R., Le, A.V., Iwase, M. (2020, MAR). Motion planner for a tetris-inspired reconfigurable floor cleaning robot. *International Journal of Advanced Robotic Systems*, 17(2), , <https://doi.org/10.1177/1729881420914441>

Wang, G., Zhao, L., Zheng, H. (2022, JUN 21). A new calibration method of stereo line-scan cameras for 2d coordinate measurement. *Frontiers in Physics*, 10, , <https://doi.org/10.3389/fphy.2022.892157>

Xu, B., Jiang, W., Shan, J., Zhang, J., Li, L. (2016, JAN). Investigation on the weighted ransac approaches for building roof plane segmentation from lidar point clouds. *Remote Sensing*, 8(1), , <https://doi.org/10.3390/rs8010005>

Xu, Y., Han, Y., Sun, Z., Gu, W., Jin, Y., Xue, X., Lan, Y. (2023, MAR). Path planning optimization with multiple pesticide and power loading bases using several unmanned aerial systems on segmented agricultural fields. *IEEE Transactions on Systems, Man, and Cybernetics: Systems*, 53(3), 1882-1894, <https://doi.org/10.1109/TSMC.2022.3205695>

Yang, T., Miro, J.V., Nguyen, M., Wang, Y., Xiong, R. (2023). Template-free non-revisiting uniform coverage path planning on curved surfaces. *IEEE/ASME Transactions on Mechatronics*, 1-9, <https://doi.org/10.1109/TMECH.2023.3275214>

Zbiss, K., Kacem, A., Santillo, M., Mohammadi, A. (2022). Automatic collision-free trajectory generation for collaborative robotic car-painting. *IEEE Access*, 10, 9950-9959, <https://doi.org/10.1109/ACCESS.2022.3144631>

Zhan, Z.-H., Zhang, J., Li, Y., Chung, H.S.-H. (2009, DEC). Adaptive particle swarm optimization. *IEEE Transactions on Systems, Man, and Cybernetics, Part B (Cybernetics)*, 39(6), 1362-1381, <https://doi.org/10.1109/TSMCB.2009.2015956>

Zhou, Y., Li, P., Ye, Z., Yue, L., Gui, L., Jiang, X., ... Liu, Y.-h. (2022, DEC). Building information modeling-based 3d reconstruction and coverage planning enabled automatic painting of interior walls using a novel painting robot in construction. *Journal of Field Robotics*, 39(8), 1178-1204, <https://doi.org/10.1002/rob.22103>